

Mixing Thermodynamics and Flory–Huggins Interaction Parameter of Polyethylene Oxide/Polyethylene Oligomeric Blends from Kirkwood–Buff Theory and Molecular Simulations

Fotis Venetsanos, Stefanos D. Anogiannakis, and Doros N. Theodorou*



Cite This: *Macromolecules* 2022, 55, 4852–4862



Read Online

ACCESS |



Metrics & More

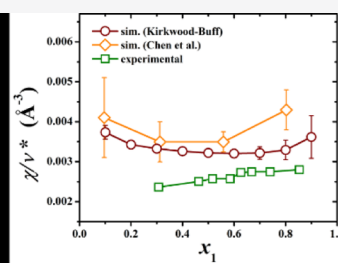
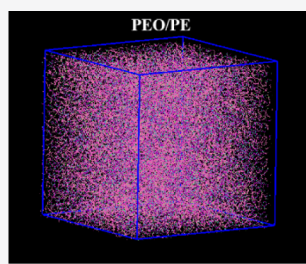


Article Recommendations



Supporting Information

ABSTRACT: In this study, we conduct a full thermodynamic analysis of polyethylene oxide/polyethylene oligomeric blends, building on the methodology introduced by Petris et al. [*J. Phys. Chem. B*, 2019, 123, 247–57], using which we contribute to the interpretation of large-scale molecular dynamics (MD) oligomeric blend simulations in the light of Kirkwood–Buff (KB) theory, featuring a composition-dependent estimation of the Flory–Huggins interaction parameter. The KB integrals are calculated from NpT MD trajectories using the particle fluctuation method. The component activity coefficients, the excess Gibbs energy of mixing, the volume, enthalpy, and entropy of mixing are extracted as functions of the mole fraction. The Flory–Huggins interaction parameter χ is estimated by interpreting the Gibbs energy of mixing in the framework of Flory–Huggins theory, and its dependence on composition is explored. A structural analysis of the studied oligomeric blends is performed to obtain the mean squared radius of gyration, the molecular pair distribution functions, and the dihedral angle distributions of the two components and is used to interpret the predicted thermodynamic properties. All the results are compared against experimental measurements and previous simulations, where available, and the agreement is found to be very good, validating our proposed methodology.



1. INTRODUCTION

Polymer blends find a diverse range of applications in materials science and engineering. Understanding how different polymer segments interact with each other, and the entropic aspects of packing chains of different constitutions and conformations in three-dimensional (3D) space, is a very important objective toward the development of new materials. One of the most important properties which expresses the affinity between the different polymer segments and plays a key role in the characterization of polymer blends and copolymers is the Flory–Huggins interaction parameter,¹ χ . The accurate estimation of the Flory–Huggins interaction parameter and, more generally, the ability to predict phase diagrams for polymer blends provide crucial information for engineering new polymeric materials.

In order to better understand χ , it is important first to describe the conditions under which it is defined. According to the Flory–Huggins theory of solutions,^{1–3} the mixing of two polymer species is modeled on a lattice, consisting of a given number of lattice sites of volume equal to a fixed reference volume, ν^* . This reference volume is defined as the volume of a segment of one of the polymer chains present, for example, of its repeating unit, or of an arbitrarily chosen reference segment. The following relationship is obeyed

$$V_i = N_i \nu^* \quad (1)$$

where V_i is the molecular volume of macromolecular species i and N_i is the number of lattice sites occupied by a chain of that species. It is evident that the Flory–Huggins theory assumes incompressibility, as the lattice is fixed and no change of volume is assumed to take place during the mixing process. In the majority of real polymer blends, the volume per monomer changes upon mixing, resulting in an excess molecular volume, which in turn characterizes the deviations from ideality and from the lattice model.⁴

The Flory–Huggins interaction parameter can be defined through the following equation^{1–3}

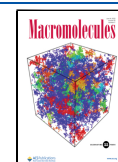
$$\frac{\Delta_{\text{mix}}G}{k_B T V} = \frac{1}{\nu^*} \left(\frac{\varphi_1}{N_1} \ln \varphi_1 + \frac{\varphi_2}{N_2} \ln \varphi_2 + \varphi_1 \varphi_2 \chi \right) \quad (2)$$

where $\Delta_{\text{mix}}G$ is the Gibbs energy of mixing, k_B and T are the Boltzmann constant and the absolute temperature, respectively, V is the total volume of the polymer blend, φ_1 and φ_2 are the volume fractions, N_1 and N_2 are the numbers of

Received: March 29, 2022

Revised: May 6, 2022

Published: May 24, 2022



segments per chain corresponding to components 1 and 2, respectively, and ν^* is the reference volume.

On the right-hand side of eq 2, the first two terms are of a combinatorial entropic origin, resulting from counting the number of ways in which chains can be placed on the fully occupied lattices representing an athermal mixture and the pure components in Flory theory,^{1,2} while the last term is enthalpic in nature. High values of χ signify unfavorable interactions between unlike segments relative to like segments, which oppose mixing; conversely, low values of χ signify favorable interactions between unlike segments relative to like segments, which favor mixing; $\chi = 0$ corresponds to the athermal case where interactions between like and unlike interactions are the same. Therefore, χ quantifies the nature of the interactions taking place between polymer species in a blend, assuming that the entropy of mixing is satisfactorily represented by the Flory expression, and governs the phase diagram of the mixture. It should be noted that χ by itself is not a lattice-independent property of the mixture. It can be transformed into one if one forms the reduced quantity χ/ν^* , which is defined as the segment interchange energy density and is often correlated with the difference in the solubility parameter between the two species.⁵

The determination of χ plays a key role in a number of problems in polymer science and is featured prominently in applications focused on the directed self-assembly of block copolymers^{6–17} for the bottom-up fabrication of micro-electronic circuits in the semiconductor and hard-drive industries, exploiting the unique ability of high- χ block copolymers to self-assemble into an abundance of patterns with narrow interfaces as a result of microphase separation. The engineering of high- χ block copolymers can provide a precise way of designing intricate shapes at micro- and nanoresolutions at a lower cost. The χ parameter has also found its way into the engineering of drug–polymer systems,^{18–20} in which a polymeric matrix is used as a means of dispersion for an amorphous drug, ensuring the drug's stability during storage and/or dissolution, requiring miscibility between the drug and polymer, and therefore aiming at low- χ drug–polymer systems.

Despite the obvious limitations generated by the approximations inherent in the theory in the context of which it is defined and the lack of accurate predictions for it from knowledge of the molecular structure alone, the Flory–Huggins parameter χ has been a very useful concept. There have been significant advances, not only in theory^{21–23} but also in computational methods for estimating χ from the molecular structure of polymers. For example, molecular simulations have been performed on miscible binary blends, computing the structure factor and then fitting χ using the random-phase approximation,^{24,25} χ has been obtained through interfacial concentration profiles from immiscible binary blend simulations;^{26,27} vapor–liquid equilibria simulations have been used to compute χ from the chemical potential;^{28,29} thermodynamic integration has also been invoked.³⁰ Nevertheless, no universal success can be claimed in determining χ as a function of a polymer blend's molecular constitution and composition from large-scale atomistic simulations. In past works,^{6–17} χ was considered to be independent of the blend molecular composition, and a constant value was accepted for it, estimated via the Hildebrand solubility parameters.⁴ However, because χ , as used in practice, absorbs all the inaccuracies stemming from the simplifying approximations invoked in

Flory theory and therefore depends on the mixture composition and on the specific property examined, the abovementioned approach provides very rough estimates, especially missing important thermodynamic phenomena occurring in dilute blends. In this work, we move past this coarse approach, aiming to break ground in the estimation of χ from large-scale atomistic simulations and explore these phenomena because we approach χ strictly as a function of blend composition.

According to eq 2, χ is directly related to the Gibbs energy of mixing. Extracting the exact Gibbs energy of mixing from molecular simulations, given a model for the molecular geometry and energetics of the components, is possible through the Kirkwood–Buff (KB) theory of solutions and its basic instruments, the KB integrals (KBIs). The KB theory was introduced in 1951³¹ and was originally developed in the grand canonical ensemble, μVT . According to the KB theory, the KBIs can be calculated by definition as integrals of the pair distribution functions of different molecules in the mixture or, equivalently, via the variances and covariance, quantifying fluctuations in local density of the individual components in the mixture.³² The KBIs can then be linked directly to thermodynamic quantities such as compressibility, partial molar volumes, or partial derivatives of the chemical potentials with respect to composition. In 1977, Ben-Naim inverted the KB theory,^{33,34} allowing the estimation of KBIs from measurable thermodynamic quantities. This offers information on both the microscopic level concerning the local structure and on the macroscopic level, for example, thermodynamic properties and compatibility between mixing components, providing a firm link between the two levels. The inversion of KB theory has since been applied extensively in various experimental works.^{35–39}

The interest in KB theory has been renewed in recent years, mainly in the field of molecular simulations. Many works have estimated KBIs via the pair distribution functions or via local particle number fluctuations within fixed subvolumes along molecular dynamics (MD) trajectories, allowing the prediction of several thermodynamic quantities for a handful of systems^{40–55} or the parameterization of atomistic force fields.^{56–61} Essential progress has been achieved, including the successful extension of KB theory, which, as mentioned previously, was originally developed in the μVT (grand canonical) ensemble, to ensembles more commonly used in MD simulations that do not involve the computational challenge of inserting and removing molecules, such as the NpT (isothermal–isobaric) and NVT (canonical) ensembles,^{40–42,62–69} while issues related to system size effects have been addressed adequately.⁴⁴

KB theory has been applied to a range of systems, including binary Lennard–Jones (LJ) mixtures,⁴³ mixtures of water with acetone,⁷⁰ urea,⁷¹ sodium chloride,⁷² methanol,⁷³ amides,⁷⁴ aromatic amino acids,⁷⁵ thiols, sulfides, and disulfides,⁷⁶ and more recently, mixtures of cyclohexane and 1-alkanol.⁴⁵ In polymer systems, a KB-derived force field has been used in the study of aqueous urea solutions of polyacrylamides.⁷⁷ An important step toward applying the KB theory for the thermodynamic analysis of chain-like molecules was made by Petris et al.⁴⁴ in the case of binary ethanol/*n*-hexane mixtures, providing a methodology that can be utilized in oligomeric blends too. This methodology was also applied by Venetsanos et al.⁴⁶ in a thermodynamic study of an ideal alkane oligomeric blend, namely 2-methylpentane/*n*-hexane mixtures.

In this work, we perform the large-scale MD simulations of the system polyethylene oxide/polyethylene (PEO/PE), a mixture of a polar and a nonpolar component with significant applications in blends and copolymers, with the aims of (a) extracting the Gibbs energy of mixing and all mixture thermodynamic properties from molecular simulations that are exact in the framework of the molecular model employed, using KB theory; (b) estimating the interaction parameter χ as a function of composition by matching the computed Gibbs energy of mixing to the Flory–Huggins expression, eq 2; and (c) elucidating aspects of packing and conformation that affect the mixing thermodynamics. We work with an oligomeric mixture for which experimental vapor–liquid equilibrium data are available for validating our predictions. Also, we invoke a united atom representation that has been used in previous simulation work, enabling useful comparisons.

The remainder of the article is structured as follows. We begin with the description of the PEO/PE oligomer binary blends we studied, the applied force field, and the parameters of the MD simulations we performed to fully equilibrate our systems and produce long enough atomistic trajectories for further processing with KB theory. Then, we present the methodology we followed to calculate the KBIs, based on the works of Cortes-Huerto et al.,^{40–42} Galata et al.,⁴³ Petris et al.,⁴⁴ and Venetsanos et al.,⁴⁶ and we proceed with the extraction of the activity coefficients of each component, the excess Gibbs energy, the excess enthalpy, and the excess entropy, and, finally, the Flory–Huggins interaction parameter, χ , as functions of composition. We then undertake a structural analysis of the systems studied, in which we present our findings concerning the molecular pair distribution functions and link them with the thermodynamic analysis we performed. Additional insight into structural parameters, in particular the mean squared radius of gyration and torsional angle distributions, is provided in the Supporting Information. Throughout our study, we compare our estimates against corresponding experimental results and data from previous simulation work, where available.

2. SYSTEMS STUDIED

We studied blends consisting of PEO and PE oligomeric chains. In Figure 1, we present the chemical constitution of the

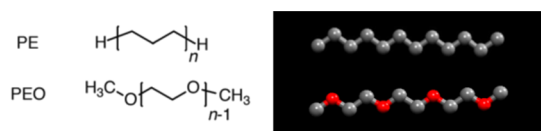


Figure 1. Chemical formulae of the oligomers studied and their corresponding united-atom representations. In our study, we simulated oligomers for $n = 4$.

two components of our blends, namely methoxy-terminated PEO trimers (triethylene glycol dimethyl ether, or triglyme) and PE hexamers (*n*-dodecane), which from this point forward we will simply call PEO and PE, respectively. We studied 11 PEO/PE blends with mole fractions $x_1 = 0, 0.1, \dots, 1$ ($x_1 = 0$ corresponds to pure PE and $x_1 = 1$ corresponds to pure PEO), at constant temperature $T = 435.26$ K and constant pressure $p = 1$ atm. All initial configurations were generated in cubic simulation boxes, applying 3D periodic boundary conditions using the amorphous builder plugin of the materials and process simulation platform.⁷⁸ Each one of these mixtures

consisted of $N = 10,000$ chains. The assigned force field was the united-atom version of the Transferable Potentials for Phase Equilibria (TraPPE),^{79,80} including a modification of the nonbonded LJ parameters and partial charges on all the united atoms belonging to PEO chains introduced by Chen et al.,²⁹ which allows improved modeling of the interactions between the PEO and PE chains, something that the original force-field parameterization was lacking as it could only model pure PEO systems accurately.

All systems were subjected to MD simulations in the isothermal–isobaric ensemble (NpT) using Large-scale Atomic/Molecular Massively Parallel Simulator software.^{81,82} The total simulation time for all the systems was 100 ns, of which the first 40 ns were considered as the equilibration stage. The integration step was 1 fs for all the simulations. The LJ 12–6 potential with the Lorentz–Berthelot combining rules⁸³ and the Coulomb potential with partial charges on the oxygen and carbon sites of PEO were used to model the intermolecular van der Waals and electrostatic interactions between pseudoatoms, respectively. The cutoff radius of the LJ potential was set equal to 14 Å for all the pairs, and analytical tail corrections⁸⁴ to the LJ interactions were applied based on the assumption of a uniform distribution of pairs beyond the truncation distance. Instead of the standard Ewald summation, we utilized the particle–particle particle–mesh method⁸⁵ to calculate the Coulomb interactions in the simulations involving PEO molecules, significantly reducing the simulation time.

At this point, we should note that, although the adopted force field provides a satisfactory modeling of the interactions at the temperature of $T = 435.26$ K and pressure $p = 1$ atm, we spotted a few inaccuracies. As displayed in Table 1, there is a

Table 1. Comparison of the Pure PEO and PE Densities, Estimated by Our MD Simulations with the Corresponding Experimental Data from Treszcjanowicz et al.⁹⁰ at $T = 435.26$ K and $p = 1$ atm

component	ρ_{sim} (kg/m ³)	ρ_{exp} (kg/m ³) ⁹⁰
PEO	851.69 ± 0.02	852.78
PE	647.87 ± 0.02	684.06

noticeable deviation between our prediction of the PE density and the corresponding experimental results, which may affect our further estimates, especially for PE-rich blends. Because of the lack of sufficient experimental data at $T = 435.26$ K, we additionally applied the same force field for the same blends that we studied but at two lower temperatures, $T = 298.15$ K and $T = 328.15$ K, estimating several thermodynamic quantities such as the excess volume and comparing them with the available experimental data.^{86–88} First of all, as we notice in Figure 2a at 298.15 K, a liquid–liquid phase separation is observed at 298.15 K, indicating that the force field overestimates the critical temperature for liquid–liquid separation of PE/PEO blends.⁸⁹ At this temperature, experimental data indicate miscibility of the two components.⁸⁶ On the contrary, at 328.15 K, no phase separation is observed but we noticed a clear deviation of the excess molar volume V_m^E from experimental data,⁸⁸ especially in PE-rich regions, as shown in Figure S1 in the Supporting Information. In addition, as we show in Figure S2, the force field slightly overestimates the density at all the compositions at this temperature.

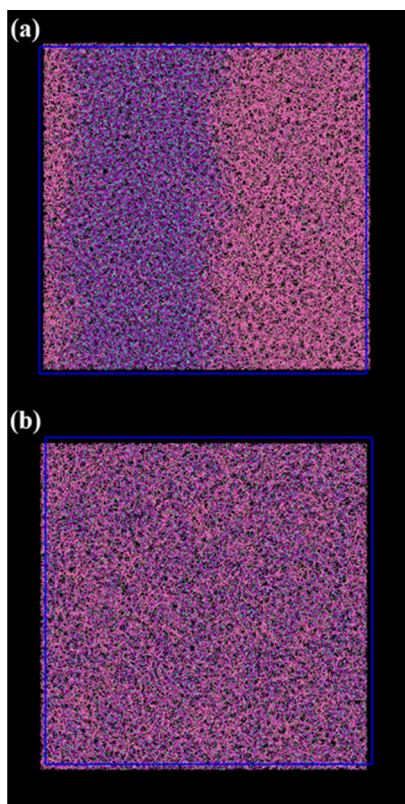


Figure 2. Visual representation of fully equilibrated equimolar PEO/PE blends at (a) 298.15 and (b) 435.26 K and constant pressure of 1 atm. PEO is represented in blue chains and PE in red chains. The snapshots were created using VMD software.^{91,92}

3. METHODOLOGY

The core of our methodology belongs to KB solution theory, which, as we have already mentioned in the Introduction, was originally developed in the μVT ensemble. A direct connection to thermodynamic properties is provided in terms of the KBIs, which can be defined as³¹

$$G_{ij}^{\mu VT} = \int_0^\infty [g_{ij}^{\mu VT}(r) - 1]4\pi r^2 dr \quad (3)$$

where $g_{ij}^{\mu VT}(r)$ is the pair distribution function defined in the grand-canonical ensemble between the two species i and j , and r is the Euclidean distance between them. The KBIs can also be expressed in terms of the particle fluctuations within a certain reference volume V of an open system³¹

$$G_{ij}^{\mu VT} = V \left(\frac{\langle N_i N_j \rangle - \langle N_i \rangle \langle N_j \rangle}{\langle N_i \rangle \langle N_j \rangle} - \frac{\delta_{ij}}{\langle N_i \rangle} \right) \quad (4)$$

where N_i and N_j are the numbers of molecules of species i and j in the reference volume V , respectively, and δ_{ij} is the Kronecker delta.

Through the extension to the NpT ensemble,^{40–43} KBIs can be defined by the relation

$$G_{ij}^{NpT} = \int_0^R [g_{ij}^{NpT}(r) - 1]4\pi r^2 dr \quad (5)$$

integrating over a region, $r < R$, over which the local mixture composition differs from the overall bulk composition.

A fundamental contribution was initially made by Krüger et al.,⁶⁶ discussing necessary corrections for the extension of KB

theory from the μVT to the NpT ensemble and for the use of a finite model system with periodic boundary conditions. This paved the way to a number of finite size-scaling correction methods, such as the works of Dawass et al.,^{65,69} in which the computation of KBIs is realized via the molecular pair distribution functions (eq 3), and of Cortes-Huerto et al.,^{40–42} who utilized the particle fluctuation expression (eq 4). The latter established a connection between the KBIs, G_{ij} , calculated by applying eq 4 in a control volume $V_c \leq V_0$, where V_0 is the total volume of the primary simulation box, and G_{ij}^∞ , which is the limiting value of G_{ij} as $V_0 \rightarrow \infty$. This connection is presented in the following equation

$$\lambda G_{ij}(\lambda) = \lambda G_{ij}^\infty (1 - \lambda^3) - \lambda^4 \frac{\delta_{ij}}{\rho_i} + \frac{\alpha_{ij}}{V_0^{1/3}} \quad (6)$$

where α_{ij} is a constant solely dependent on intensive thermodynamic system properties such as density and temperature, ρ_i is the number density of species i , and $\lambda = (V_c/V_0)^{1/3}$.

Based on the corrections introduced by Cortes-Huerto et al.,^{40–42} Galata et al.⁴³ developed a methodology for the calculation of KBIs in LJ mixtures via the particle fluctuation method, based on eq 6, by superimposing a 3D grid in cubic simulation boxes, thereby partitioning the simulation boxes into smaller cells. These smaller cells are open systems, capable of mass transfer among them under designated volume and temperature, meaning that they are governed by the μVT ensemble. Therefore, the KBIs can be calculated in each smaller cell, separately, for a variety of grids. A characteristic parameter, λ , defined as $\lambda = (V_{\text{cell}}/V_{\text{min}})^{1/3}$ is corresponding to each grid, where V_{min} is the minimum volume of the simulation box in the course of the NpT ensemble simulation and V_{cell} is the volume of a cell in the grid. The average value over all cells (N_{cells} in number) is

$$G_{ij}(\lambda) = \frac{1}{N_{\text{cells}}} \sum_{k=1}^{N_{\text{cells}}} G_{ij,k}(\lambda) \quad (7)$$

Petris et al.⁴⁴ extended the aforementioned methodology of Galata et al.⁴³ in order to include more chain-like binary mixtures, such as *n*-hexane/ethanol. They introduced a segment-based method, in which each molecule is considered as a chain of segments. Each segment is centered on a discrete united atom, amounting to a specific fraction of the molecule, proportional to the united atom's molar mass. The segment-based method was also used in a thermodynamic analysis of 2-methylpentane/*n*-heptane binary mixtures by Venetsanos et al.⁴⁶ In the present work, each PEO and PE molecule is viewed as an assemblage of 12 segments centered at the centers of their backbone united atoms. A higher molar mass of the segment, constituting a larger fraction of its molecule, yields a greater contribution to fluctuations.

In Figure S3, we plot $\lambda G_{ij}(\lambda)$ versus λ as obtained from an equilibrated MD simulation of the mixture at 435.26 K. We observe a linear behavior for lower λ values ($\lambda \leq 0.3$). This behavior is expected from eq 6 and is similar to the one observed in the works of Cortes-Huerto et al.,^{40–42} Galata et al.,⁴³ Petris et al.,⁴⁴ and Venetsanos et al.⁴⁶ In this linear regime, we can conduct a linear fit and determine the limiting value G_{ij}^∞ from the slope according to eq 6. Because this part is very prone to system size effects, we performed several trials to make sure that there are no significant system size effects

between systems consisting of $N = 10,000$ and $N = 20,000$ molecules in total with various compositions, allowing us to work only with the smaller system in order to reduce the computational cost.

4. RESULTS AND DISCUSSION

In this section, we present the results of our study for the PEO/PE oligomer blends using the particle fluctuation method, as proposed by Cortes-Huerta et al.,^{40–42} in combination with the segment-based method proposed by Petris et al.⁴⁴ The section is divided into two subsections, Section 4.1 and Section 4.2, of which the first subsection corresponds to the application of the KB theory, providing a full thermodynamic analysis of the oligomeric blends we study, calculating the activity coefficients of the two components, the excess Gibbs energy, the excess enthalpy, and the excess entropy as functions of composition, and finally, the Flory–Huggins interaction parameter as a function of composition directly from the Gibbs energy of mixing. The second subsection focuses on a structural analysis of the systems studied, presenting the molecular pair distribution functions at various compositions.

4.1. Application of the Kirkwood-Buff Theory. As mentioned earlier, we have available 60 ns of fully equilibrated trajectories of the oligomer blends studied. For the implementation of the KB theory in the post-processing, we utilized the first and the last 25 ns to provide us with two discrete statistical samples, with the 10 ns in between acting as a buffer zone so as to ensure the best possible independence between our samplings. Error bars are obtained from averaging over the two different subtrajectories and are omitted in specific figures where they are very small in comparison to the size of the symbols.

4.1.1. Activity Coefficients. Activity coefficients are thermodynamic factors expressing deviations from ideal solutions in a chemical mixture. The activity coefficients are linked by definition to the chemical potential, μ . Let us consider the chemical potential, μ_i^{id} , of component i in an ideal mixture

$$\mu_i^{\text{id}} = \mu_i^* + k_{\text{B}}T \ln x_i \quad (8)$$

where μ_i^* is the chemical potential of pure component i at the temperature and pressure of the mixture, and x_i is the mole fraction of component i in the mixture. The abovementioned definition can be generalized for nonideal mixtures using the following relation

$$\mu_i = \mu_i^* + k_{\text{B}}T \ln \gamma_i x_i \quad (9)$$

γ_i is the activity coefficient of component i , defined using the pure component i at the mixture temperature and pressure as a reference state.

Differentiation of eq 9 provides us with the following differential equation

$$x_i \left(\frac{\partial \ln \gamma_i}{\partial x_i} \right)_{T,p} = \frac{x_i}{k_{\text{B}}T} \left(\frac{\partial \mu_i}{\partial x_i} \right)_{T,p} - 1 \quad (10)$$

The chemical potential derivative on the right-hand side of eq 10 can be calculated via the KBIs through the relation below

$$\frac{1}{k_{\text{B}}T} \left(\frac{\partial \mu_i}{\partial x_i} \right)_{T,p} = \frac{\rho}{x_i[\rho_1 + \rho_2 + \rho_1 \rho_2 (G_{11}^{\infty} + G_{22}^{\infty} - 2G_{12}^{\infty})]} \quad (11)$$

where $\rho_1 = N_1/\langle V \rangle$ and $\rho_2 = N_2/\langle V \rangle$ are the number densities of components 1 and 2, respectively, $\rho = \rho_1 + \rho_2$, and $\langle V \rangle$ is the average NpT simulation volume. As we described in the Methodology Section, the KBIs, G_{11}^{∞} , G_{12}^{∞} , and G_{22}^{∞} are calculated using the segment-based method proposed by Petris et al.⁴⁴

The activity coefficients for each substance can now be estimated by solving the abovementioned differential equation. Although we could extract the activity coefficients following a numerical integration scheme, we decided, in order to achieve the best possible accuracy, to solve eq 10 analytically, fitting to the values of $1/k_{\text{B}}T(\partial \mu_i/\partial x_i)_{T,p}$ with a seventh degree polynomial

$$P(x_i) = a_7 x_i^7 + a_6 x_i^6 + a_5 x_i^5 + a_4 x_i^4 + a_3 x_i^3 + a_2 x_i^2 + a_1 x_i + a_0 \quad (12)$$

where α_n are real constants.

As an example, in Figure S4, we present the very good fits of the polynomial we mentioned above to the reduced first derivatives of the chemical potential for species 1 (PEO) and 2 (PE).

Therefore, eq 10 is transformed into the following equation

$$\left(\frac{\partial \ln \gamma_i}{\partial x_i} \right)_{T,p} = a_7 x_i^7 + a_6 x_i^6 + a_5 x_i^5 + a_4 x_i^4 + a_3 x_i^3 + a_2 x_i^2 + a_1 x_i + a_0 - \frac{1}{x_i} \quad (13)$$

which can be easily integrated analytically to provide us with the values of the activity coefficients, γ_1 and γ_2 . Before we proceed, we must clarify that we performed two separate polynomial fits for the two components, and then we verified that the resulting functions are thermodynamically consistent, validating successfully the two fitted functions of γ_1 and γ_2 via the Gibbs–Duhem equation

$$x_1 d \ln \gamma_1 + x_2 d \ln \gamma_2 = 0 \quad (14)$$

In Figure 3, we plot our estimates for the activity coefficients, γ_1 and γ_2 , as functions of the mole fraction, x_1 . To validate our methodology, we compare our results with the experimental data of Treszczanowicz et al.,⁹⁰ and we provide further comparison with the simulation work of Chen et al.,²⁹ which employs the same force field as we do. The activity coefficient values in both the experimental vapor–liquid equilibrium experiments of Treszczanowicz et al.⁹⁰ and the Gibbs ensemble Monte Carlo simulations of Chen et al.²⁹ are extracted from the corresponding p_{xy} phase diagrams by applying the generalized Raoult's law⁹³

$$\gamma_1 x_1 \phi_1^s p_1^s = \gamma_1 \phi_{p,1} p \quad (15)$$

where p_1^s is the saturation pressure of component 1, PEO, γ_1 is the mole fraction of component 1 in the vapor phase, $\phi_{p,1}$ is the fugacity coefficient of component 1 in the vapor, ϕ_1^s is the fugacity coefficient of pure 1 saturated vapor, and p is the pressure. The fugacity coefficient is set as equal to unity for each composition, which is justified due to low pressure with very small deviations, within a margin of ± 0.08 kPa, reported

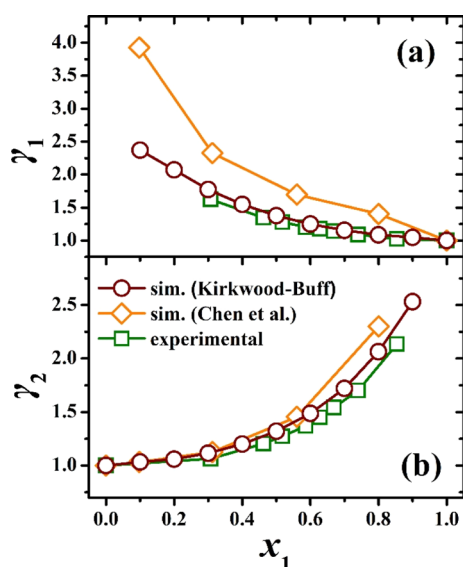


Figure 3. Activity coefficients γ_1 (a) and γ_2 (b) plotted vs the mole fraction of PEO, x_1 , for PEO/PE oligomeric blends as calculated from the KB theory, being compared to experimental data from Trespaczanowicz et al.⁹⁰ and Gibbs ensemble Monte Carlo simulation data from Chen et al.²⁹ at $T = 435.26$ K and $p = 1$ atm.

by Trespaczanowicz et al.⁹⁰ The fugacity coefficients of the pure components in their saturated vapor state were also set equal to unity, in view of the low vapor pressures. Thus, the following simpler equation was used to process literature data

$$\gamma_i x_i p_i^s = y_i p \quad (16)$$

A very good agreement is observed between our estimates and the corresponding experimental findings.⁹⁰ The deviations between our simulation results and the estimates of Chen et al.²⁹ probably stem from the fact that smaller systems were studied in their Gibbs ensemble Monte Carlo simulations, in comparison to the much larger systems used in our present MD simulations.

For infinite dilution, the excess component's activity coefficient converges to unity ($x_i \rightarrow 1$, $\gamma_i \rightarrow 1$), while for all other compositions, both γ_1 and γ_2 have a value greater than unity ($\gamma_i > 1$), denoting positive deviations from ideal solution behavior for the oligomeric blends studied, an indication of unfavorable interactions between chains of different species in relation to same species interactions. The abovementioned will consequently result in a positive excess Gibbs energy and excess enthalpy, as will be shown in the following section.

4.1.2. Excess Gibbs Energy, Excess Enthalpy, and Excess Entropy. Now that we have accurately estimated the activity coefficients, we can easily calculate the excess Gibbs energy per molecule for the PEO/PE blends by applying the following relation

$$G^E = k_B T (x_1 \ln \gamma_1 + x_2 \ln \gamma_2) \quad (17)$$

In Figure 4, we present the excess molar Gibbs energy, $G_m^E = N_A G^E$, where N_A is the Avogadro's number, as a function of x_1 , calculated using eq 17. As in the case of the activity coefficients, we compare our results with the experimental data of Trespaczanowicz et al.⁹⁰ and with the simulation work of Chen et al.²⁹

Reasonable agreement is displayed between our estimates and the experimental data;⁹⁰ our simulations overestimate the

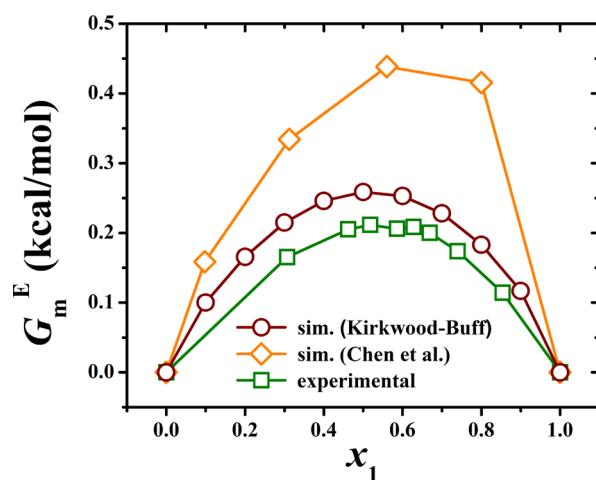


Figure 4. Excess molar Gibbs energy, G_m^E , plotted vs the PEO mole fraction, x_1 , for PEO/PE oligomeric blends, as calculated directly from the activity coefficients, compared to experimental data from Trespaczanowicz et al.⁹⁰ and Gibbs ensemble Monte Carlo simulation data from Chen et al.²⁹ at $T = 435.26$ K and $p = 1$ atm.

nonideality of the mixture somewhat. This is quite possibly an effect of the force field used. As mentioned in the **Systems Studied Section**, there is an underestimation of the PE density linked directly to the force field, making it a probable primary cause for deviations observed across the range of thermodynamic estimations; these deviations are largest in PE-rich blends. Significant deviations are seen between our estimates and the simulation results of Chen et al.²⁹ Worthy of mention is that the excess molar Gibbs energy is slightly skewed to the right in the experimental data⁹⁰ and in a much more prevalent manner in the simulation data of Chen et al.²⁹ This asymmetry is not observed in our estimates. Although it could indicate an increased nonideality for blends richer in PEO, there might be simpler explanations. As we notice in Figure 4, there are significantly fewer experimental values in the PE-rich regions, that is, $x_1 < 0.5$ as opposed to the PEO-rich regions, that is, $x_1 > 0.5$, making it difficult to reach a definite conclusion. Regarding the simulation data of Chen et al.,²⁹ it is possible that the skewness and overall significant deviations from the rest of the data, both our simulation estimates and the experimental ones, are once again a result mainly of the small system size used in their Gibbs ensemble Monte Carlo simulations, with the force field possibly partaking in these deviations in a secondary role. As expected, the excess Gibbs energy is a purely positive quantity, signifying the positive deviations from the ideal behavior discussed in the **Activity Coefficients Section**.

In order to provide a complete thermodynamic analysis of the PEO/PE blends studied, we also calculated the excess enthalpy, H_m^E , and the excess entropy, S_m^E , of the blends. The excess enthalpy is calculated directly from our MD simulations as

$$H^E = H^{\text{blend}} - x_1 H_1^{\text{pure}} - x_2 H_2^{\text{pure}} \quad (18)$$

where H^{blend} is the enthalpy of the blend, and H_1^{pure} and H_2^{pure} are the enthalpies of pure PEO and PE components, respectively, all quantities being expressed per molecule.

Finally, the excess entropy can be calculated from the definition of the Gibbs energy as

$$TS^E = H^E - G^E \quad (19)$$

In Figure 5, we plot the excess molar energies G_m^E , $H_m^E = N_A H^E$, and $TS_m^E = N_A TS^E$, as obtained from our MD

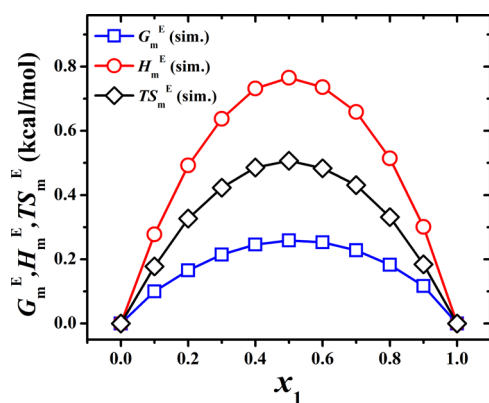


Figure 5. Excess molar Gibbs energy, excess molar enthalpy, and excess molar entropy, plotted versus the PEO mole fraction, x_1 , for PEO/PE oligomeric blends at $T = 435.26$ K and $p = 1$ atm.

simulations. No further experimental or simulation data were available, except for the molar excess Gibbs energy, which was already presented in Figure 4 previously.

The excess molar enthalpy, H_m^E , is positive, indicating an endothermic mixing process, as already anticipated in relation to our activity coefficient estimates shown in Figure 5. The excess molar entropy, S_m^E , is positive, indicating a higher entropy of mixing than for an ideal system.

4.1.3. Flory–Huggins Interaction Parameter. In this section, we present our estimates of the Flory–Huggins interaction parameter, implementing our methodology based on the combination of KB and Flory–Huggins theories. Therefore, we first calculate the Gibbs energy of mixing

$$\Delta_{\text{mix}}G = G^E + \Delta_{\text{mix}}G^{\text{id}} \quad (20)$$

where G^E is the excess Gibbs energy, as calculated in the previous section, and $\Delta_{\text{mix}}G^{\text{id}} = k_B T(x_1 \ln x_1 + x_2 \ln x_2)$. The Gibbs energy of mixing (also shown in Figure S3) is negative at all blend compositions, exhibiting positive deviations from the ideal behavior as expected from our previous findings.

Having calculated the Gibbs energy of mixing, the Flory–Huggins interaction parameter can now be extracted from eq 2, solving for χ . The volume fractions φ_i are here approximated by

$$\varphi_i = \frac{n_i M_i / \rho_{i,\text{pure}}}{n_1 M_1 / \rho_{1,\text{pure}} + n_2 M_2 / \rho_{2,\text{pure}}} \quad i = 1, 2 \quad (21)$$

where n_i is the number of i -type chains, M_i is their molar mass, and $\rho_{i,\text{pure}}$ is the density of the pure component i . Note from the way we estimate volume fractions φ_i that the Flory–Huggins model assumes incompressibility, which, as mentioned in the Introduction, is not valid for our polymer blend because in our case there is a positive deviation from ideality, which results in a positive excess volume of up to 1% relative to ideal mixing. A reference volume of $\nu^* = 100 \text{ \AA}^3$ was used for mapping to Flory theory, and the chain segments corresponding to the two oligomer species were defined as $N_i = V_i / \nu^*$. The value of ν^* has been chosen here as equal to the value used in the simulations of Chen et al.²⁹ to facilitate comparisons.

In Figure 6, we present our estimates of the Flory–Huggins interaction parameter, χ , and we compare them with the

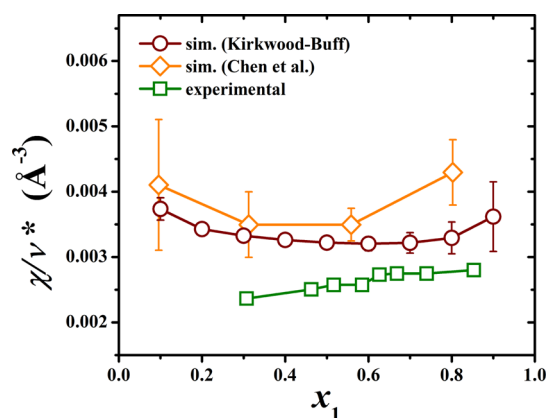


Figure 6. The Flory–Huggins interaction parameter reduced by the reference volume, χ/ν^* , plotted versus the PEO mole fraction, x_1 , for PEO/PE oligomeric blends, compared to experimental data from Treszczanowicz et al.⁹⁰ and Gibbs ensemble Monte Carlo simulation data from Chen et al.²⁹ at $T = 435.26$ K and $p = 1$ atm.

corresponding experimental data of Treszczanowicz et al.⁹⁰ and Gibbs ensemble Monte Carlo simulation data of Chen et al.²⁹ at $T = 435.26$ K and $p = 1$ atm.

For blends richer in PE, our estimates tend to be closer to the simulation results of Chen et al.,²⁹ while in PEO-rich solutions, our estimates lie in between the experimental data⁹⁰ and the Gibbs ensemble Monte Carlo data of Chen et al.²⁹ As in the case of the excess Gibbs energy, which was explored in the previous section and from which χ is directly derived, this deviation from experimental data can be explained as an effect of the force field we apply. As demonstrated in the Systems Studied Section, there is an underestimation of the PE density, which gets carried over to the blend simulations and is prevalent in systems of higher PE concentration, leading to an increase in total volume. This increased volume is also providing a longer chain segment corresponding to PE (larger N_2), contributing, according to eq 2, to an underestimation of the entropic part of the Gibbs energy of mixing, which in turn results in an overestimation of the enthalpic part, leading therefore to an increased χ estimate. Concerning the shape of the curve, there is an agreement between our estimates and the Gibbs ensemble Monte Carlo data,²⁹ as a nearly parabolic convex symmetry is observed.

The positive, but relatively low value of χ signifies weak repulsive interactions between the PEO and PE chains, but, due to the low molecular weights of both oligomeric chains, no liquid/liquid separation is evident, resulting in a single liquid phase throughout the entire composition range,⁴ as shown, for example, in Figure 2b for the equimolar PE/PEO blend. We also note increased values of χ for dilute blends, which is typical of fitting Flory theory to experimental blend data.⁹⁴

4.2. Molecular Pair Distribution Functions. In Figure 7, we plot the molecular pair distribution functions between the centers of mass of the oligomeric chains for various mole fractions. At long distances, all molecular pair distribution functions tend to 1, which corresponds to the regime where there is no long-range order. In Figure 7a, where $g_{11}(r)$ is plotted, we notice a single peak for each composition. This peak is moving to shorter distances, increasing its height and

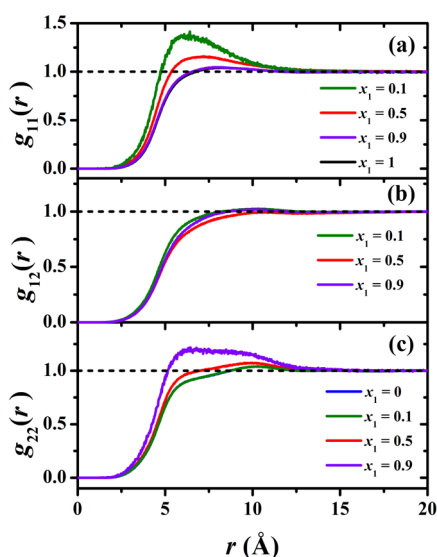


Figure 7. Molecular pair distribution functions, (a) $g_{11}(r)$, (b) $g_{12}(r)$, and (c) $g_{22}(r)$ of PEO/PE binary mixtures for PEO mole fractions $x_1 = 0, 0.1, 0.5, 0.9$, and 1 at $T = 435.26$ K and $p = 1$ atm.

sharpness as x_1 decreases. This indicates that PEO chains approach each other more and more upon mixing with PE chains, which is in agreement with the positive deviations from ideal solution behavior of the mixtures revealed by the thermodynamic analysis we performed in the previous sections. A more peculiar situation is observed in Figure 7c, where $g_{22}(r)$ is plotted. Here, two different peaks can be distinguished instead of a single sharp peak. In PE dilute blends ($x_1 = 0.9$), the first peak, which appears at shorter distances, is clearly more elevated than the second one, which appears at longer distances; as PE concentration increases, however, the second peak in $g_{22}(r)$ becomes dominant. In order to provide a physical insight into the existence of two peaks in the molecular $g_{22}(r)$ we isolated and inspected visually a few PE chain pairs which contribute to either the first or the second peaks.

In Figure 8a–d, we show four characteristic PE chain pairs which contribute to the first peak for $x_1 = 0.1$ at $r = 6.4$ Å. We

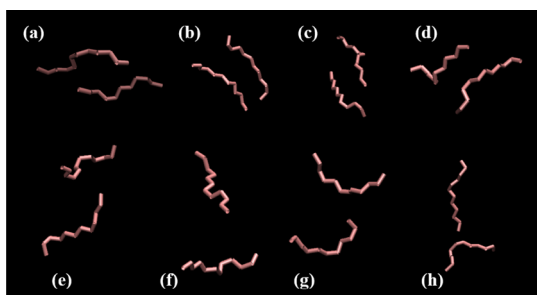


Figure 8. Visual representation of eight PE chain pairs. Pairs (a–d) contribute to the first peak while (e–h) contribute to the second peak of the $g_{22}(r)$ molecular pair distribution function at $x_1 = 0.9$, as shown in Figure 7c. All the snapshots were created using VMD software.^{91,92}

observe that the chains in each pair are oriented almost parallel to each other. On the other hand, as shown in Figure 8e–h, where we show four PE chain pairs which contribute to the second peak in $g_{22}(r)$, at $r = 10.3$ Å, the relative orientation of the chains in each pair seems to be random. In order to check

quantitatively the abovementioned finding, we have calculated the orientational correlation function S , defined as

$$S = \frac{3\langle \cos^2 \theta_{ij} \rangle - 1}{2} \quad (22)$$

where θ_{ij} is the angle between the end-to-end vectors of two chains i and j belonging to a pair, and the bracket corresponds to an average over all available chain pairs contributing to either the first or the second peak. Indeed, for the first peak in $g_{22}(r)$, we found $S \approx 0.11$, indicating a weak preference for parallel orientation between chain pairs, while for the second peak, $S \approx 0$ indicating that there is no preferential orientation between the chain pairs, both results verifying our observables. We can thus conclude that increasing the PEO content of the blend pushes PE chains into close encounters where their backbones tend to run parallel to each other.

Finally, in Figure 7b, where the cross distribution function $g_{12}(r)$ is plotted versus r for various mole fractions, we observe that all curves are suppressed relative to 1, especially the one that corresponds to the equimolar system. This reveals the unfavorable interactions between nonpolar PE and polar PEO chains, which manifest themselves in positive deviations of the blend mixing thermodynamics from ideal solution behavior, as analyzed in the previous sections.

Apart from the analysis of the molecular pair distribution functions, a more in-depth structural study of the PEO/PE oligomeric blends has been undertaken and is presented in the Supporting Information, focusing on the radius of gyration and torsion angle distributions and extracting important information about the stiffness of chains at various blend compositions.

5. SUMMARY AND CONCLUSIONS

We have presented a full thermodynamic analysis of the PEO/PE oligomeric blend system, introducing an original expansion of the methodology developed by Petris et al.,⁴⁴ in which we combine the KB and Flory–Huggins theories, making possible a straightforward estimation of the Flory–Huggins interaction parameter as a function of blend composition from large-scale MD oligomeric blend simulations. In particular, we have computed the activity coefficients, several excess thermodynamic properties and, more importantly, the Gibbs energy of mixing as a function of blend composition, via the KB theory of solutions, following the works of Cortes-Huerto et al.^{40–42} and Petris et al.⁴⁴ and providing the necessary extensions in order to be able to estimate the Flory–Huggins interaction parameter as a function of blend composition. Our thermodynamic estimates were compared to corresponding experimental⁹⁰ and simulation²⁹ data, where available, the latter using the same force field as our simulations. Overall, good agreement with our estimates was obtained, validating the accuracy of our proposed methodology. We have also revealed the blend's positive deviations from ideal solution behavior (interactions between unlike components being less favorable than interactions between like components), as exhibited by the activity coefficients, the excess Gibbs energy, and the endothermic enthalpy of mixing. Having calculated the Gibbs energy of mixing, we have estimated the Flory–Huggins interaction parameter, χ , confirming both the positive deviations from ideality and the endothermic nature of the system in good agreement with the corresponding experimental data and other simulation results. Interpreting our computed Gibbs energy of mixing in the framework of Flory's

thermodynamics leads to a χ which stays pretty much constant over intermediate compositions but rises when the mixture becomes very dilute in either component.

In addition to our thermodynamic predictions, we have also analyzed the structure of the PE/PEO oligomeric blends, providing direct links between the atomistic chain packing and conformation and the thermodynamics of mixing. We have shown that the mean squared radius of gyration, molecular pair distribution functions, and dihedral angle distributions are interconnected with macroscopic properties. We encountered interesting phenomena stemming from the flexibility of the PEO chains, mainly due to the $-\text{O}-\text{C}-\text{C}-\text{O}-$ dihedral angle and the relative stiffness of the PE chains (see [Supporting Information](#)). One of our most interesting findings was the noticeable stiffening of PEO chains and the minor coiling of PE chains upon mixing. Another noteworthy attribute is the presence of two distinct peaks in the PE molecular pair distribution function, which change in different ways when the blend composition is varied. As the blend becomes leaner in PE, there is an increasing tendency for PE chains to form closely spaced pairs with their backbones parallel to each other.

The successful implementation of our methodology paves the way to further expanding our knowledge to quantify the dependence of the Flory–Huggins interaction parameter on temperature and chain length in large-scale MD simulations of polymer blends. In addition, it forms a basis for predicting the mixing thermodynamics of polymer blends from simulation, bearing in mind that a reliable force field, able to describe interactions between components in the mixture accurately, is absolutely necessary.

■ ASSOCIATED CONTENT

SI Supporting Information

The Supporting Information is available free of charge at <https://pubs.acs.org/doi/10.1021/acs.macromol.2c00642>.

Force field parameters used in the simulations; excess molar volume, plotted versus the mole fraction of PEO, for PEO/PE oligomeric blends and comparison with corresponding experimental results; density plotted versus the mole fraction of PEO, for PEO/PE oligomeric blends and comparison with corresponding experimental results; application of the segment-based method for the estimation of KBIs in the equimolar PEO/PE blend; examples of the polynomial fits to the reduced first derivatives of the chemical potential, $1/k_{\text{B}}T(\partial\mu_i/\partial x_i)_{T,p}$; molar Gibbs energy of mixing, molar enthalpy of mixing, and molar entropy of mixing, plotted versus the PEO mole fraction, for PEO/PE oligomer binary mixtures and comparison with the corresponding thermodynamic predictions for ideal solutions; mean squared radius of gyration; and dihedral angle distributions ([PDF](#))

■ AUTHOR INFORMATION

Corresponding Author

Doros N. Theodorou – School of Chemical Engineering, National Technical University of Athens, Athens 15780, Greece; orcid.org/0000-0002-4763-9739; Email: doros@central.ntua.gr

Authors

Fotis Venetsanos – School of Chemical Engineering, National Technical University of Athens, Athens 15780, Greece

Stefanos D. Anogiannakis – School of Chemical Engineering, National Technical University of Athens, Athens 15780, Greece; orcid.org/0000-0001-9766-2243

Complete contact information is available at: <https://pubs.acs.org/10.1021/acs.macromol.2c00642>

Author Contributions

The manuscript was written through the equal contributions of all the authors. All the authors have given approval to the final version of the manuscript.

Notes

The authors declare no competing financial interest.

■ ACKNOWLEDGMENTS

This research is co-financed by Greece and the European Union (European Social Fund-ESF) through the Operational Program “Human Resources Development, Education and Lifelong Learning” in the context of the project “Reinforcement of Postdoctoral Researchers—2nd Cycle” (MIS-5033021), implemented by the State Scholarships Foundation (IKY). Scienomics SARL is gratefully acknowledged for making their software available to us through the Scienomics Group of Scientific Excellence program. This work was supported by computational time granted from the National Infrastructures for Research and Technology S.A. (GRNET S.A.) in the National HPC facility—ARIS—under project IDs pr008038_thin and pr009027_thin.

■ REFERENCES

- (1) Flory, P. J. *Principles of Polymer Chemistry*; Cornell University, 1953.
- (2) Flory, P. J. Thermodynamics of High Polymer Solutions. *J. Chem. Phys.* **1942**, *10*, 51–61.
- (3) Huggins, M. L. Solutions of Long Chain Compounds. *J. Chem. Phys.* **1941**, *9*, 440.
- (4) Rubinstein, M.; Colby, R. H. *Polymer Physics*; Oxford University, 2003.
- (5) Van Krevelen, D. W. Coal constitution and solvent extraction. *Fuel* **1965**, *44*, 229.
- (6) Stoykovich, M. P.; Müller, M.; Kim, S. O.; Solak, H. H.; Edwards, E. W.; de Pablo, J. J.; Nealey, P. F. Directed Assembly of Block Copolymer Blends into Nonregular Device-Oriented Structures. *Science* **2005**, *308*, 1442–1446.
- (7) Stoykovich, M. P.; Kang, H.; Daoulas, K. C.; Liu, G.; Liu, C.-C.; de Pablo, J. J.; Müller, M.; Nealey, P. F. Directed Self-Assembly of Block Copolymers for Nanolithography: Fabrication of Isolated Features and Essential Integrated Circuit Geometries. *ACS Nano* **2007**, *1*, 168–175.
- (8) Darling, S. B. Directing the self-assembly of block copolymers. *Prog. Polym. Sci.* **2007**, *32*, 1152–1204.
- (9) Welander, A. M.; Kang, H.; Stuen, K. O.; Solak, H. H.; Müller, M.; de Pablo, J. J.; Nealey, P. F. Rapid Directed Assembly of Block Copolymer Films at Elevated Temperatures. *Macromolecules* **2008**, *41*, 2759–2761.
- (10) Nagpal, U.; Müller, M.; Nealey, P. F.; de Pablo, J. J. Free Energy of Defects in Ordered Assemblies of Block Copolymer Domains. *ACS Macro Lett.* **2012**, *1*, 418–422.
- (11) Li, W.; Nealey, P. F.; de Pablo, J. J.; Müller, M. Defect Removal in the Course of Directed Self-Assembly is Facilitated in the Vicinity of the Order-Disorder Transition. *Phys. Rev. Lett.* **2014**, *113*, 168301.
- (12) Aissou, K.; Mumtaz, M.; Fleury, G.; Portale, G.; Navarro, C.; Cloutet, E.; Brochon, C.; Ross, C. A.; Hadziioannou, G. Sub-10 nm Features Obtained from Directed Self-Assembly of Semicrystalline Polycarbosilane-Based Block Copolymer Thin Films. *Adv. Mater.* **2014**, *27*, 261–265.

- (13) Li, W.; Müller, M. Directed self-assembly of block copolymers by chemical or topographical guiding patterns: Optimizing molecular architecture, thin-film properties, and kinetics. *Prog. Polym. Sci.* **2016**, *54*, 47–75.
- (14) Kayer, F.; Fleury, G.; Thongkham, S.; Navarro, C.; Martin-Vaca, M.; Bourissou, D. Microphase Separation of Polybutyrolactone-Based Block Copolymers with Sub-20 nm Domains. *Macromolecules* **2018**, *51*, 6534–6541.
- (15) Li, D.; Zhou, C.; Xiong, S.; Qu, X.-P.; Craig, G. S. W.; Nealey, P. F. Enhanced microphase separation of thin films of low molecular weight block copolymer by the addition of an ionic liquid. *Soft Matter* **2019**, *15*, 9991–9996.
- (16) Cummins, C.; Mantione, D.; Cruciani, F.; Pino, G.; Demazy, N.; Shi, Y.; Portale, G.; Hadziioannou, G.; Fleury, G. Rapid Self-Assembly and Sequential Infiltration Synthesis of High χ Fluorine-Containing Block Copolymers. *Macromolecules* **2020**, *53*, 6246–6254.
- (17) Cummins, C.; Pino, G.; Mantione, D.; Fleury, G. Engineering block copolymer materials for patterning ultra-low dimensions. *Mol. Syst. Des. Eng.* **2020**, *5*, 1642–1657.
- (18) Zhao, Y.; Inbar, P.; Chokshi, H. P.; Malick, A. W.; Choi, D. S. Prediction of the Thermal Phase Diagram of Amorphous Solid Dispersions by Flory–Huggins Theory. *J. Pharm. Sci.* **2011**, *100*, 3196–3207.
- (19) Tian, Y.; Booth, J.; Meehan, E.; Jones, D. S.; Li, S.; Andrews, G. P. Construction of Drug–Polymer Thermodynamic Phase Diagrams Using Flory–Huggins Interaction Theory: Identifying the Relevance of Temperature and Drug Weight Fraction to Phase Separation within Solid Dispersions. *Mol. Pharmaceutics* **2013**, *10*, 236–248.
- (20) Potter, C. B.; Davis, M. T.; Albadarin, A. B.; Walker, G. M. Investigation of the Dependence of the Flory–Huggins Interaction Parameter on Temperature and Composition in a Drug–Polymer System. *Mol. Pharmaceutics* **2018**, *15*, 5327–5335.
- (21) Schweizer, K. S. Analytic PRISM theory of structurally asymmetric polymer blends and copolymers. *Macromolecules* **1993**, *26*, 6050–6067.
- (22) Freed, K. F.; Dudowicz, J. Influence of short chain branching on the miscibility of binary polymer blends: application to polyolefin mixtures. *Macromolecules* **1996**, *29*, 625–636.
- (23) White, R. P.; Lipson, J. E. G. Free volume, cohesive energy density, and internal pressure as predictors of polymer miscibility. *Macromolecules* **2014**, *47*, 3959–3968.
- (24) Heine, D.; Wu, D. T.; Curro, J. G.; Grest, G. S. Role of intramolecular energy on polyolefin miscibility: isotactic polypropylene/polyethylene blends. *J. Chem. Phys.* **2003**, *118*, 914–924.
- (25) Jaramillo, E.; Wu, D. T.; Grest, G. S.; Curro, J. G. Anomalous mixing behavior of polyisobutylene/polypropylene blends: molecular dynamics simulation study. *J. Chem. Phys.* **2004**, *120*, 8883–8886.
- (26) Groot, R. D.; Warren, P. B. Dissipative particle dynamics: bridging the gap between atomistic and mesoscopic simulation. *J. Chem. Phys.* **1997**, *107*, 4423–4435.
- (27) Chremos, A.; Nikoubashman, A.; Panagiotopoulos, A. Z. Flory-Huggins parameter χ , from binary mixtures of Lennard-Jones particles to block copolymer melts. *J. Chem. Phys.* **2014**, *140*, 054909.
- (28) Chen, Q. P.; Chu, J. D.; DeJaco, R. F.; Lodge, T. P.; Siepmann, J. I. Molecular Simulation of Olefin Oligomer Blend Phase Behavior. *Macromolecules* **2016**, *49*, 3975–3985.
- (29) Chen, Q. P.; Xie, S.; Foudazi, R.; Lodge, T. P.; Siepmann, J. I. Understanding the Molecular Weight Dependence of χ and the Effect of Dispersity on Polymer Blend Phase Diagrams. *Macromolecules* **2018**, *51*, 3774–3787.
- (30) Zhang, W.; Gomez, E. D.; Milner, S. T. Predicting Flory-Huggins χ from simulations. *Phys. Rev. Lett.* **2017**, *119*, 017801.
- (31) Kirkwood, J. G.; Buff, F. P. The statistical mechanical theory of solutions. *J. Chem. Phys.* **1951**, *19*, 774–777.
- (32) Ben-Naim, A. *Molecular Theory of Solutions*; Oxford University Press: Oxford, New York, 2006.
- (33) Ben-Naim, A. Inversion of the Kirkwood–Buff theory of solutions: Application to the water–ethanol system. *J. Chem. Phys.* **1977**, *67*, 4884–4890.
- (34) Nain, A. K. Inversion of the Kirkwood–Buff Theory of Solutions: Application to Tetrahydrofuran + Aromatic Hydrocarbon Binary Liquid Mixtures. *J. Solution Chem.* **2008**, *37*, 1541–1559.
- (35) Perera, A.; Sokolić, F.; Almásy, L.; Westh, P.; Koga, Y. On the evaluation of the Kirkwood–Buff integrals of aqueous acetone mixtures. *J. Chem. Phys.* **2005**, *123*, 024503.
- (36) Perera, A.; Sokolić, F.; Almásy, L.; Koga, Y. Kirkwood–Buff integrals of aqueous alcohol binary mixtures. *J. Chem. Phys.* **2006**, *124*, 124515.
- (37) Shulgin, I. L.; Ruckenstein, E. The Kirkwood–Buff Theory of Solutions and the Local Composition of Liquid Mixtures. *J. Phys. Chem. B* **2006**, *110*, 12707–12713.
- (38) Almásy, L.; Jancsó, G.; Cser, L. Applications of SANS to the determination of Kirkwood–Buff integrals in liquid mixtures. *Appl. Phys. A: Mater. Sci. Process.* **2002**, *74*, s1376–s1378.
- (39) Dey, R.; Verma, R.; Nautiyal, T.; Soni, N. K.; Pandey, J. D. Determination of Kirkwood–Buff integrals of multicomponent liquid mixtures from the speed of sound. *Phys. Chem. Liq.* **2009**, *47*, 287–295.
- (40) Cortes-Huerta, R.; Kremer, K.; Potestio, R. Kirkwood–Buff integrals in the thermodynamic limit from small-sized molecular dynamics simulations. *J. Chem. Phys.* **2016**, *145*, 141103.
- (41) Heidari, M.; Kremer, K.; Potestio, R.; Cortes-Huerta, R. Fluctuations, Finite-Size Effects and the Thermodynamic Limit in Computer Simulations: Revisiting the Spatial Block Analysis Method. *Entropy* **2018**, *20*, 222.
- (42) Heidari, M.; Kremer, K.; Potestio, R.; Cortes-Huerta, R. Finite-size integral equations in the theory of liquids and the thermodynamic limit in computer simulations. *Mol. Phys.* **2018**, *116*, 3301–3310.
- (43) Galata, A. A.; Anogiannakis, S. D.; Theodorou, D. N. Thermodynamic Analysis of Lennard-Jones binary mixtures using Kirkwood–Buff theory. *Fluid Phase Equilib.* **2018**, *470*, 25–37.
- (44) Petris, P. C.; Anogiannakis, S. D.; Tzounis, P.-N.; Theodorou, D. N. Thermodynamic analysis of n-hexane–ethanol binary mixtures using the Kirkwood–Buff theory. *J. Phys. Chem. B* **2019**, *123*, 247–257.
- (45) Almasi, M. Study of molecular interactions and preferential solvation in binary mixtures of cyclohexane and (C5–C10) 1-alkanol by Kirkwood–Buff integrals. *Fluid Phase Equilib.* **2019**, *489*, 1–7.
- (46) Venetsanos, F.; Anogiannakis, S. D.; Theodorou, D. N. Thermodynamic Analysis of Oligomeric Blends by Applying the Kirkwood–Buff Theory of Solutions. *J. Phys.: Conf. Ser.* **2021**, *2090*, 012079.
- (47) Dawass, N.; Krüger, P.; Schnell, S. K.; Moulto, O. A.; Economou, I. G.; Vlugt, T. J. H.; Simon, J.-M. Kirkwood–Buff Integrals Using Molecular Simulation: Estimation of Surface Effects. *Nanomaterials* **2020**, *10*, 771.
- (48) Miyaji, M.; Radola, B.; Simon, J.-M.; Krüger, P. Extension of Kirkwood–Buff theory to solids and its application to the compressibility of fcc argon. *J. Chem. Phys.* **2021**, *154*, 164506.
- (49) Krüger, P. Validity of the compressibility equation and Kirkwood–Buff theory for crystalline matter. *Phys. Rev. E* **2021**, *103*, L061301.
- (50) Pierce, V.; Kang, M.; Aburi, M.; Weerasinghe, S.; Smith, P. E. Recent Applications of Kirkwood–Buff Theory to Biological Systems. *Cell Biochem. Biophys.* **2008**, *50*, 1–22.
- (51) Kang, M.; Smith, P. E. Preferential interaction parameters in biological systems by Kirkwood–Buff theory and computer simulation. *Fluid Phase Equilib.* **2007**, *256*, 14–19.
- (52) Ben-Naim, A. Theoretical aspects of self-assembly of proteins: A Kirkwood–Buff-theory approach. *J. Chem. Phys.* **2013**, *138*, 224906.
- (53) Shimizu, S.; Stenner, R.; Matubayasi, N. Gastrophysics: Statistical thermodynamics of biomolecular denaturation and gelation from the Kirkwood–Buff theory towards the understanding of tofu. *Food Hydrocolloids* **2017**, *62*, 128–139.
- (54) Gee, M. B.; Smith, P. E. Kirkwood–Buff theory of molecular and protein association, aggregation, and cellular crowding. *J. Chem. Phys.* **2009**, *131*, 165101.

- (55) Ploetz, E. A.; Karunaweera, S.; Benteinitis, N.; Chen, F.; Dai, S.; Gee, M. B.; Jiao, Y.; Kang, M.; Kariyawasam, N. L.; Naleem, N.; Weerasinghe, S.; Smith, P. E. Kirkwood–Buff-Derived Force Field for Peptides and Proteins: Philosophy and Development of KBFF20. *J. Chem. Theory Comput.* **2021**, *17*, 2964–2990.
- (56) Fyta, M. Structural and technical details of the Kirkwood–Buff integrals from the optimization of ionic force fields: focus on fluorides. *Eur. Phys. J. E: Soft Matter Biol. Phys.* **2012**, *35*, 21.
- (57) Gee, M. B.; Cox, N. R.; Jiao, Y.; Benteinitis, N.; Weerasinghe, S.; Smith, P. E. A Kirkwood–Buff Derived Force Field for Aqueous Alkali Halides. *J. Chem. Theory Comput.* **2011**, *7*, 1369–1380.
- (58) Fyta, M.; Netz, R. R. Ionic force field optimization based on single-ion and ion-pair solvation properties: Going beyond standard mixing rules. *J. Chem. Phys.* **2012**, *136*, 124103.
- (59) Mercadante, D.; Milles, S.; Fuertes, G.; Svergun, D. I.; Lemke, E. A.; Gräter, F. Kirkwood–Buff Approach Rescues Overcollapse of a Disordered Protein in Canonical Protein Force Fields. *J. Phys. Chem. B* **2015**, *119*, 7975–7984.
- (60) Naleem, N.; Benteinitis, N.; Smith, P. E. A Kirkwood–Buff derived force field for alkaline earth halide salts. *J. Chem. Phys.* **2018**, *148*, 222828.
- (61) Weerasinghe, S.; Gee, M. B.; Kang, M.; Benteinitis, N.; Smith, P. E. Developing Force Fields from the Microscopic Structure of Solutions: The Kirkwood–Buff Approach. In *Modeling Solvent Environments: Applications to Simulations of Biomolecules*; Feig, M., Ed.; Wiley-VCH: Weinheim, 2010; pp 55–76.
- (62) Kobayashi, T.; Reid, J. E. S. J.; Shimizu, S.; Fyta, M.; Smiatek, J. The properties of residual water molecules in ionic liquids: a comparison between direct and inverse Kirkwood–Buff approaches. *Phys. Chem. Chem. Phys.* **2017**, *19*, 18924–18937.
- (63) Mukherji, D.; van der Vegt, N. F. A.; Kremer, K.; Delle Site, L. Kirkwood–Buff Analysis of Liquid Mixtures in an Open Boundary Simulation. *J. Chem. Theory Comput.* **2012**, *8*, 375–379.
- (64) Ganguly, P.; van der Vegt, N. F. A. Convergence of Sampling Kirkwood–Buff Integrals of Aqueous Solutions with Molecular Dynamics Simulations. *J. Chem. Theory Comput.* **2013**, *9*, 1347–1355.
- (65) Dawass, N.; Krüger, P.; Schnell, S. K.; Bedeaux, D.; Kjelstrup, S.; Simon, J. M.; Vlugt, T. J. H. Finite-size effects of Kirkwood–Buff integrals from molecular simulations. *Mol. Simul.* **2018**, *44*, 599–612.
- (66) Krüger, P.; Schnell, S. K.; Bedeaux, D.; Kjelstrup, S.; Vlugt, T. J. H.; Simon, J.-M. Kirkwood–Buff Integrals for Finite Volumes. *J. Phys. Chem. Lett.* **2013**, *4*, 235–238.
- (67) Dawass, N.; Krüger, P.; Simon, J.-M.; Vlugt, T. J. H. Kirkwood–Buff integrals of finite systems: shape effects. *Mol. Phys.* **2018**, *116*, 1573–1580.
- (68) Krüger, P.; Vlugt, T. J. H. Size and shape dependence of finite-volume Kirkwood–Buff integrals. *Phys. Rev. E* **2018**, *97*, 051301.
- (69) Dawass, N.; Krüger, P.; Schnell, S. K.; Simon, J.-M.; Vlugt, T. J. H. Kirkwood–Buff integrals from molecular simulation. *Fluid Phase Equilib.* **2019**, *486*, 21–36.
- (70) Weerasinghe, S.; Smith, P. E. Kirkwood–Buff derived force field for mixtures of acetone and water. *J. Chem. Phys.* **2003**, *118*, 10663.
- (71) Weerasinghe, S.; Smith, P. E. A Kirkwood–Buff derived force field for mixtures of urea and water. *J. Phys. Chem. B* **2003**, *107*, 3891–3898.
- (72) Weerasinghe, S.; Smith, P. E. A Kirkwood–Buff derived force field for sodium chloride in water. *J. Chem. Phys.* **2003**, *119*, 11342.
- (73) Weerasinghe, S.; Smith, P. E. A Kirkwood–Buff Derived Force Field for Methanol and Aqueous Methanol Solutions. *J. Phys. Chem. B* **2005**, *109*, 15080–15086.
- (74) Kang, M.; Smith, P. E. A Kirkwood–Buff derived force field for amides. *J. Comput. Chem.* **2006**, *27*, 1477–1485.
- (75) Ploetz, E. A.; Smith, P. E. A Kirkwood–Buff force field for the aromatic amino acids. *Phys. Chem. Chem. Phys.* **2011**, *13*, 18154–18167.
- (76) Benteinitis, N.; Cox, N. R.; Smith, P. E. A Kirkwood–Buff Derived Force Field for Thiols, Sulfides, and Disulfides. *J. Phys. Chem. B* **2009**, *113*, 12306–12315.
- (77) Nayar, D.; Folberth, A.; van der Vegt, N. F. A. Molecular origin of urea driven hydrophobic polymer collapse and unfolding depending on side chain chemistry. *Phys. Chem. Chem. Phys.* **2017**, *19*, 18156–18161.
- (78) Scienomics. *MAPS Platform*, version 4.1.1: France, 2016.
- (79) Martin, M. G.; Siepmann, J. I. Novel Configurational-Bias Monte Carlo Method for Branched Molecules. Transferable Potentials for Phase Equilibria. 2. United-Atom Description of Branched Alkanes. *J. Phys. Chem. B* **1999**, *103*, 4508–4517.
- (80) Stubbs, J. M.; Potoff, J. J.; Siepmann, J. I. Transferable Potentials for Phase Equilibria. 6. United-Atom Description for Ethers, Glycols, Ketones, and Aldehydes. *J. Phys. Chem. B* **2004**, *108*, 17596–17605.
- (81) Plimpton, S. Fast Parallel Algorithms for Short-Range Molecular Dynamics. *J. Comput. Phys.* **1995**, *117*, 1–19.
- (82) Thompson, A. P.; Aktulga, H. M.; Berger, R.; Bolintineanu, D. S.; Brown, W. M.; Crozier, P. S.; in 't Veld, P. J.; Kohlmeyer, A.; Moore, S. G.; Nguyen, T. D.; Shan, R.; Stevens, M. J.; Tranchida, J.; Trott, C.; Plimpton, S. J. LAMMPS - a flexible simulation tool for particle-based materials modeling at the atomic, meso, and continuum scales. *Comp. Phys. Comm.* **2022**, *271*, 108171.
- (83) Maitland, G. C.; Rigby, M.; Smith, E. B.; Wakeham, W. A. *Intermolecular Forces: Their Origin and Determination*; Oxford University Press, 1981.
- (84) Wood, W. W.; Parker, F. R. Monte Carlo Equation of State of Molecules Interacting with the Lennard-Jones Potential. I. A Supercritical Isotherm at about Twice the Critical Temperature. *J. Chem. Phys.* **1957**, *27*, 720–733.
- (85) Hockney, R. W.; Eastwood, J. W. *Computer Simulation Using Particles*; IOP Publishing Ltd. Bristol: England, 1988.
- (86) Treszczanowicz, T.; Benson, G. C.; Lu, B. C.-Y. Excess Volumes for Binary Mixtures Formed by 2,5,8,11-Tetraoxadodecane or 2,5,8,11,13-Pentaoxadodecane with Homologous *n*-Alkanes. *Thermochim. Acta* **1990**, *168*, 95–102.
- (87) Treszczanowicz, T.; Benson, G. C.; Lu, B. C.-Y.; Benjamin, L. C.-Y. Excess Enthalpies for Binary Mixtures Formed by 2,5,8,11-Tetraoxadodecane with Homologous *n*-Alkanes. *Thermochim. Acta* **1990**, *168*, 95–102.
- (88) Rivas, M. A.; Iglesias, T. P.; Pereira, S. M.; Banerji, N. On the permittivity and density measurements of binary systems of {triglyme + (*n*-nonane or *n*-dodecane)} at various temperatures. *J. Chem. Thermodyn.* **2005**, *37*, 61–71.
- (89) Treszczanowicz, T.; Cieślak, D. Liquid + liquid Equilibria in (a Dimethyl Ether of a Polyethylene Glycol + an *n*-Alkane). *J. Chem. Thermodyn.* **1993**, *25*, 661–665.
- (90) Treszczanowicz, T.; Lu, B. C.-Y. Isothermal vapour-liquid equilibria for 11 examples of (an ether + a hydrocarbon). *J. Chem. Thermodyn.* **1986**, *18*, 213–220.
- (91) Humphrey, W.; Dalke, A.; Schulten, K. VMD - Visual Molecular Dynamics. *J. Mol. Graphics* **1996**, *14*, 33–38.
- (92) <http://www.ks.uiuc.edu/Research/vmd/>.
- (93) Tassios, D. *Chemical Engineering Thermodynamics*; Springer-Verlag, 1993.
- (94) Gujrati, P. D. Composition dependence of chi from neutron scattering, compressibility, and a purely interaction chi. *J. Chem. Phys.* **2000**, *112*, 4806.